Cell Transplantation, Vol. 21, pp. 2587–2602, 2012

0963-6897/12 $90.00 + .00
DOI: http://dx.doi.org/10.3727/096368912X653228
E-ISSN 1555-3892
www.cognizantcommunication.com

Human Induced Pluripotent Stem Cells Improve Stroke Outcome and Reduce Secondary Degeneration in the Recipient Brain

Jérôme Polentes,* Pavla Jendelova,† Michel Cailleret,* Holger Braun,‡ Nataliya Romanyuk,† Philippe Tropel,*§ Marion Brenot,* Valerie Itier,*¶ Christine Seminatore,* Kathrin Baldauf,‡ Karolina Turnovcova,† Daniel Jirak,# Marius Teletin,** Julien Côme,* Johana Tournois,* Klaus Reymann,‡ Eva Sykova,† Stéphane Viville,§** and Brigitte Onteniente*

*I-Stem, INSERM UMR861, UEVE, Evry Cedex, France
†Institute of Experimental Medicine, ASCR, Department of Neuroscience and Center for Cell Therapy and Tissue Repair, Prague, Czech Republic
‡Leibniz Institut für Neurobiologie, Magdeburg, Germany
§IGBMC, Dpt Biologie Cellulaire & Développement, Illkirch-Graffenstaden Cedex, France
¶Université Paris-Est Créteil, Créteil Cedex, France
#Institute for Clinical and Experimental Medicine, Prague, Czech Republic
**Faculté de Médecine, Centre Hospitalier Universitaire, Strasbourg Cedex, France

Human induced pluripotent stem cells (hiPSCs) are a most appealing source for cell replacement therapy in acute brain lesions. We evaluated the potential of hiPSC therapy in stroke by transplanting hiPSC-derived neural progenitor cells (NPCs) into the postischemic striatum. Grafts received host tyrosine hydroxylase-positive afferents and contained developing interneurons and homotopic GABAergic medium spiny neurons that, with time, sent axons to the host substantia nigra. Grafting reversed stroke-induced somatosensory and motor deficits. Grafting also protected the host substantia nigra from the atrophy that follows disruption of reciprocal striatonigral connections. Graft innervation by tyrosine hydoxylase fibers, substantia nigra protection, and somatosensory functional recovery were early events, temporally dissociated from the slow maturation of GABAergic neurons in the grafts and innervation of substantia nigra. This suggests that grafted hiPSC-NPCs initially exert trophic effects on host brain structures, which precede integration and potential pathway reconstruction. We believe that transplantation of NPCs derived from hiPSCs can provide useful interventions to limit the functional consequences of stroke through both neuroprotective effects and reconstruction of impaired pathways.

Key words: Cell replacement therapy; Cerebral ischemia; Reprogramming; Intracerebral transplantation; Neurovascular lesions

INTRODUCTION

Despite decades of academic and industrial research, cerebrovascular diseases continue to thwart the attempts of developing neuroprotective treatments and remain a leading cause of death and long-term disability worldwide (49). The proof of principle of stem cell (SC) therapy in stroke has been provided at experimental level with a wide array of cell sources that, not exhaustively, include neural progenitors from fetal and adult neural tissues, mesenchymal SCs from bone marrow (BMSCs) or umbilical cord blood, peripheral blood cells, immortalized cell lines, and embryonic SCs (ESCs) of rodent, primate, and human origin (5,7,27,35,47,53). Encouraging experimental data have fostered Phase I–II trials, so far published with BMSCs and neural cell lines (3,24).

Induced pluripotent SCs (iPSCs) (45) have added a unique source to the panel of available resources for SC therapy. IPSCs possess the cardinal features of ESCs, pluripotency and unlimited self-renewal, which are definitive assets for the large-scale and standardized production of therapeutic products. In addition, hiPSCs have the potential to overcome immune rejection with human leukocyte antigen (HLA)-specific cells (23,34). On the iPSCs "dark side," reprogramming can leave epigenetic and genetic

Received November 16, 2011; final acceptance May 25, 2012. Online prepub date: August 10, 2012.
Address correspondence to Brigitte Onteniente, I-STEM; INSERM UMR861/UEVE/AFM, 5 rue Henri Desbrueres, F-91030 Evry Cedex, France. Tel: +33-1-6990-8538; Fax: +33-1-6990-8521; E-mail: brigitte.onteniente@inserm.fr

modifications (17,21,28,48) with still unknown functional repercussions. As a result, the fate and effects of iPSC-derived neural progeny must be thoroughly investigated in preclinical models before therapies based on hiPSCs are proposed to clinicians (10).

In contrast with the unprecedented therapeutic options offered by iPSCs, illustrations of therapeutic transplantation applications are still scarce. Thus far, two reports have described iPSC transplantation in stroke models, firstly, confirming their ability to form teratoma after intracerebral transplantation (20) and, secondly, showing a reduction of stroke-induced motor dysfunction after subdural transplantation with fibrin glue (9). Both reports were performed with undifferentiated mouse iPSCs, leaving the potential of human neural derivatives unexplored.

In this study, hiPSC-derived neural progenitor cells (NPCs) were used to define their ability to reverse stroke-induced functional and structural impairments after intracerebral transplantation. Our results show that hiPSC-NPCs not only rescue sensorimotor and motor functions but protect remote areas connected with the lesioned site from atrophy. Mismatches in the kinetics of functional and structural events suggest the existence of sequential mechanisms, independent, then dependent, on homotopic cell replacement and reconstruction of lost pathways.

MATERIALS AND METHODS

Validation of hiPSC Lines and Neural Induction

The I-Stem-Strasbourg (I-S)hiPSC lines were derived from MRC5 and IMR90 human fetal lung fibroblasts (ATCC, Manassas VA, USA) transduced with the pSin-EF2-octamer-binding transcription factor 4 (Oct4)-Pur, pSin-EF2-sex-determining region Y Box 2 (Sox2)-Pur, pSin-EF2-Nanog-Pur, and pSin-EF2-Lin28-Pur13 plasmids from Addgene (Cambridge, MA, USA) according to Yu et al. (52). Viruses were produced by Vectalys (Labège, France; MOI between 7 and 23). The culture medium (Dulbecco's modified Eagle medium containing 10% fetal bovine serum) was progressively modified over 1 week to serum-free hESC medium containing 20 ng/ml basic fibroblast growth factor (bFGF; R&D Systems, Minneapolis, MN, USA). Transduced fibroblasts were seeded onto mouse embryonic feeder cells and grown in hESC medium. Colonies with ESC morphology appeared after 3–6 weeks and were clonally expanded for 5 weeks with mechanical passage every 5–7 days. Seven colonies from IMR90 and five from MRC5 cultures were selected on a morphological basis and validated for the expression of hESC self-renewal genes and surface markers and for pluripotency through embryoid bodies and teratoma formation before commitment into the neural lineage. Data were compared to hESC lines that included the SA001 (XY; Cellartis AB, Gothenburg, Sweden), H9 (XX; WiCell, Madison, WI, USA), and CCTL14 (XX; Masaryk University, Brno, Czech Republic) lines.

Quantitative PCR Analysis

Real-time quantitative (q) PCR (Primer list in Table 1) was performed with the RNeasy microkit (Qiagen, France) and Superscript III reverse transcriptase (Invitrogen, France) on 0.5 μg cDNA. Normalization was achieved against glyceraldehyde 3-phosphate dehydrogenase (GAPDH) RNA using the ΔΔCt method for quantification (ABI-Prism Software, Applied Biosystems).

Flow Cytometry Analysis

Flow cytometry (FACSCalibur Flow Cytometer, BD Biosciences) analysis of the ESC-specific cell surface markers stage-specific embryonic antigen-1 (SSEA-1) [mouse IgM coupled to allophycocyanin (APC)], SSEA-4 (mouse IgG3 coupled to Alexa-Fluor 488), and TRA-1-81 [mouse IgM coupled to phycoerythrin (PE)] was performed

Table 1. List of Primers Used for qRT-PCR

Gene	Forward	Reverse	Size
OCT3/4	CTTGCTGCAGAAGTGGGTGGAGGAA	CTGCAGTGTGGGTTTCGGGCA	168
NANOG	CAAAGGCAAACAACCCACTT	TCTGCTGGAGGCTGAGGTAT	158
SOX2	ACAGCAAATGACAGCTGCAAA	TCGGCATCGCGGTTTTT	67
KLF4	TATGACCCACACTGCCAGAA	TGGGAACTTGACCATGATTG	110
LIN28	GGCAGTGGAGTTCACCTTT	GCTTCTGCATGCTCTTTCCT	123
DNMT	CCAATCCTGGAGGCTATCCG	ACTGGGGTGTCAGAGCCAT	152
CRIPTO	AAGATGGCCCGCTTCTCTTAC	AGATGGACGAGCAAATTCCTG	108
CK18	TGAGACGTACAGTCCAGTCCT	GCTCCATCTGTAGGGCGTAG	114
KDR	AGCGATGGCCTCTTCTGTAA	ACACGACTCCATGTTGGTCA	172
SOX17	CCTGGGTTTTTGTTGTTGCT	GCTGTTTTGGGACACATTCA	206
AFP	ACTGCAATTGAGAAACCCACTGGAGATG	CGATGCTGGAGTGGGCTTTTTGTGT	192
GAPDH	ATGGGGAAGGTGAAGGTCGGAG	TCGCCCCACTTGATTTTGGAGG	266

DNMT, DNA methyltransferase; CK18, cytokeratin 18; KDR, kinase insert domain protein receptor; AFP, α-fetoprotein; GAPDH, glyceraldehyde 3-phosphate dehydrogenase.

on the selected clones and on SA001 with appropriate isotype controls (all antibodies from BD Biosciences).

Embryoid Bodies Formation

Embryoid bodies (EBs) were formed after collagenase dissociation (1 mg/ml, Invitrogen) and seeding on ultra-low attachment plates (Nunc, Dutscher) for 3–6 weeks without bFGF. EBs were analyzed after 4 and 14 days by qPCR for markers of the three germ layers.

Karyotype Analysis

I-ShiPSCs were harvested for metaphase chromosomes at 70% confluence. G-banding chromosome analysis was performed with the Wright/Giemsa (Merck) technique after colchicine (20 mg/ml, Eurobio) incubation, hyptonic shock (KCl 0.057 M), and fixation with Carnoy's solution (3:1 methanol/acetic acid). Analysis was performed with the Ikaros software (MetaSystems, Altussheim). Multicolor fluorescent in situ hybridization (mFISH) were performed at passages 18 (both lines) and at p56 (I-I90) or p59 (I-M5) with the cocktail painting Probe Cy5 B-tect detection kit and Isis software (MetaSystems, Altussheim).

Teratoma Formation

Pluripotency was further investigated with the teratoma test performed in nonobese diabetic/severe combined immunodeficient mice (NOD/SCID; Charles River, France) after subcutaneous injection of 2×10^6 cells, with anatomo-pathological analysis 2 months postinjection.

Neural Induction

Early neural precursors (ENPs) were produced in low-attachment cultures in the presence of Noggin (R&D Systems), the transforming growth factor-β pathway inhibitor SB431542 (Tocris Biosci.), bFGF (10 μg/ml, Preprotech), and human brain-derived growth factor (hBDNF; 20 μg/ml, R&D Systems) (8). NPCs were produced from ENPs in the presence of 20 ng/ml hBDNF for 7 days. Expression levels of pluripotency and neural cell markers were quantified by qPCR and flow cytometry, respectively. Fluorescence-activated cell sorting (FACS) antibodies included anti-Nanog, TRA-1-60 and SSEA4 (eBioscience), CD29, CD15 (SSEA1), CD56 (neural cell adhesion molecule, NCAM), and βIII-tubulin (all from BD Pharmingen), along with unconjugated mouse primary antibodies against nestin and neurofilament 70 kDa (NF70) (Abcam), secondary rat anti-mouse IgG conjugated with fluorescein isothiocyanate (FITC; eBioscience), and secondary donkey anti-rabbit IgG conjugated with APC (Jackson ImmunoResearch Labs).

Voltage clamp was used to record potassium outward current in the whole-cell configuration (20–25°C) filtered at 3.3 kHz, using the HEKA data acquisition/analysis system. Pipettes (5–7 MΩ) were pulled from borosilicate glass with P97-sutter and filled with (mM): KCl 155, $MgCl_2$ 2, $CaCl_2$ 1, HEPES 10, and EGTA 10 (pH 7.3). Cells were maintained in (mM): NaCl 150, $CaCl_2$ 3, KCl 2.5, $MgCl_2$ 1, HEPES 10 (pH 7.6). Steps of +10 mV from the holding voltage Vh-90 mV were applied during 50 ms to record A-type calcium current (IA), 500 ms to record delayed rectifying current (IDR), and 50 ms to record voltage-gated sodium current (INa).

Experimental Surgery

All animal experimentation was performed in compliance with European ethical guidelines (86/609/EEC). Adult male (280 g) Sprague–Dawley rats (Charles River; $n=187$) were anesthetized (1–2% isoflurane/30% oxygen/75% nitrous oxide) before receiving a 90-min middle cerebral artery occlusion MCAO (30) with a heparinized 4.0 nylon monofilament (Doccol Corporation; (40) SPPK5; MyDesign MCAO suture PK5; coating length 2–3 mm, tip diameter 0.35 ± 0.02 mm). Rectal temperature was maintained between 36.7°C and 37.5°C with a homeothermic blanket (Harvard Apparatus). Three animals died during MCAO surgery, either during anesthesia ($n=1$) or at reperfusion ($n=2$). One week after MCAO, animals were randomly distributed into four groups: Control (MCAO nongrafted; $n=35$), I-I90-NPC ($n=29$), I-M5-NPC ($n=29$), and SA001-NPC ($n=15$). A group of nonlesioned/nongrafted animals ($n=12$) was also used for quantification of substantia nigra (SN) volumes. Grafted animals received a stereotaxic injection of 1 μl of culture medium (Control) alone or containing 100,000 NPCs from I-I90, I-M5, or SA001 (coordinates from bregma A-P: 0.5 mm; Lat: 2 mm; D-V: 5.5 mm) with a needle inclination of 15° to reach the lesion cavity in the lateral quadrant of the striatum. Three additional animals died during this procedure (two during anesthesia, one from bleeding at removal of the needle), resulting in a final distribution of Control ($n=34$), I-I90-NPC ($n=28$), I-M5-NPC ($n=29$), SA001-NPC ($n=14$). Animals were immunosuppressed with a daily injection of 10 mg kg^{-1} cyclosporine A (Sandimmun, Novartis) starting the day before transplantation for 2 months. Body weight was followed daily.

Behavioral Analysis

All behavioral tests were conducted by investigators blinded to the experimental conditions. To avoid habituation of animals to repeated behavioral investigation (18), I-I90-NPC-grafted animals were used for the adhesive removal test and I-IM5-NPC-grafted animals for the staircase test. Animals grafted with I-I90-, I-M5- and SA001-NPCs were used for the apomorphin-induced rotation test. For the adhesive removal test (I-I90: $n=28$; Nongrafted: $n=19$ at the start of experiment), a sticky colored paper dot (12 mm diameter) was placed on the

rat left palm and fingers, and the time to remove the dot was measured. Rats were pretrained for 4 days before MCAO and were tested three times a week. The staircase test was performed with sucrose pellets (Campden Instruments Ltd.; three pellets on each side). Animals (I-M5: $n=29$; Nongrafted: $n=15$ at the start of the experiment) were food-deprived to 85% of their normal weight and trained for 3 weeks (two trials per day, 5 days a week) before MCAO and three times a week after transplantation. Scores indicate the number of pellets grasped by the paw contralateral to the lesion. The apomorphin-induced rotation test (motor dysfunction, pharmacological) was performed on grafted (I-I90: $n=28$; I-M5: $n=29$; SA001: $n=14$ at the start of the experiment) and on nongrafted ($n=34$) animals. Turns were counted during 30 min following intraperitoneal injection of 1 mg/kg apomorphin–HCl (Sigma). Deficits were quantified using the formula modified from Arvidsson et al (2): Score = IspiCyl + (2× IpsiItself) − ContrCyl − (2×ContrItself), where IpsiCyl: rotation ipsilateral to the lesion around central cylinder, IpsiItself: rotation ipsilateral on itself, ContrCyl: rotation contralateral to the lesion around the central cylinder, ContrItself: rotation contralateral on itself. Neurological severity scores (NSS) were performed on all groups up to 4 months postgrafting (39). Function was graded on a 0 (normal) to 10 (severely impaired) scale.

Tissue Processing

Rats were anesthetized with 150 mg/kg sodium pentobarbital before intracardiac perfusion with 4% paraformaldehyde phosphate-buffered to pH 7.4. Brains were postfixed overnight in the same fixative solution and cryoprotected with 30% sucrose for 48 h. Thirty-micrometer-thick cryostat sections were serially collected with a Leica CM cryostat. Immunohistochemistry was performed with rabbit polyclonal antibodies to human nestin (Chemicon, AB5922), glial fibrillary acidic protein (GFAP; Sigma, G9269), dopamine- and cAMP-regulated neuronal phosphoprotein (DARPP-32; Santa Cruz Biotech., sc-21601), paired box protein 6 (Pax6; Covance, PRB-278P), unspecific tyrosine hydroxylase (TH; Jacques Boy, 208020234), Ki67 (Abcam, ab833), and neuron-specific class III beta-tubulin (TUJ1; Covance, MMS-435P) and with mouse IgG antibodies to human nuclei (HNA; Chemicon, MAB1281), human mitochondria (MTCO2, Abcam, 3298), Oct4 (Santa Cruz Biotech., SC-5279), human NCAM (SantaCruz Biotech., sc-106), and microtubule-associated protein 2 (MAP2; Sigma, M1406). Secondary antibodies were Alexa488- or Alexa555-labeled (A11001 and A21428, respectively, Invitrogen). IB4 labeling was performed with isolectin *Griffonia simplicifolia* (GS)-IB4 biotin conjugate (Invitrogen, I2141) and revealed with Alexa647 (Jackson Labs., 016-600-084). DAPI (4′,6-diamidino-2-phenylindole) was used to visualize the nuclei. Colorimetric immunohistochemistry was performed using a Discovery XT (Ventana) staining automate. Controls were performed with the corresponding isotype when available or with secondary antibodies only. Observations were made using a Zeiss Axioplan microscope, and image analysis was performed with ImageJ (http://rsb.info.nih.gov/ij). Confocal microscopy was done on a Zeiss LSM Pascal Exciter microscope. Ki67-, DARPP-32- and TH-positive neuron counts were performed with unbiased stereological evaluation on three (Ki67) or six (DARPP-32) consecutive 30-µm-thick sections at 120-µm interval. TH-positive neuron counts were performed from level –4.8 to –6.3 from bregma, independently of the SN volume. Volumes were calculated using the FreeD software (1).

Magnetic Resonance Imaging (MRI)

MRI was performed using a 4.7-T Bruker spectrometer equipped with a custom made surface coil. A T2-weighted turbospin echo sequence rapid acquisition with relaxation enhancement [RARE; repetition time (TR) = 3,000 ms, effective echo time (TE) = 36.0 ms, turbo factor = 8, number of acquisitions (AC) = 8, field of view = 3.5 cm, matrix = 256×256, slice thickness = 0.85 mm, acquisition time = 9′36″] was used.

Statistical Analysis

Data are expressed as means ± standard deviation. Statistical analyses were performed using the JMP software (SAS). A value of $p<0.05$ was considered significant.

Data were analyzed using one-way or repeated-measures ANOVA and Student's *t* test, with Bonferroni–Dunn post hoc test.

RESULTS

Production of hiPSC and Transplants

The two I-ShiPSC lines, I-I90 (XX) (25) and I-M5 (XY), were validated by comparison to the SA001 (Cellartis AB) and H9 (WiCell) hESC lines (Figs. 1 and 2). I-ShiPSC presented all characteristics of pluripotent SCs, including morphology (Fig. 1A, B), expression of hESC-specific markers (Fig. 1C–E), methylation pattern on *OCT4* and *NANOG* promoters (Fig. 1F), and karyotype stability (Fig. 1G, H). I-ShiPSCs were able to produce EBs (Fig. 2A, B) with hESC-like gene expression (Fig. 2C, D) and formed teratoma after implantation into the immunodeficient mouse (Fig. 2E–H). Early neural precursors (ENPs) were derived using the dual-small body size mothers against decapentaplegic (SMAD) inhibition protocol described for hESCs (Fig. 3). Rosette-like ENPs (Fig. 3A) contained Nanog (Fig. 3B), Pax6 (Fig. 3C), and no Oct4 (Fig. 3C). RT-PCR revealed elevated levels of Nanog mRNA in I-ShiPSC-ENPs (Table 2). I-M5-ENPs additionally exhibited elevated Sox2 mRNA contents

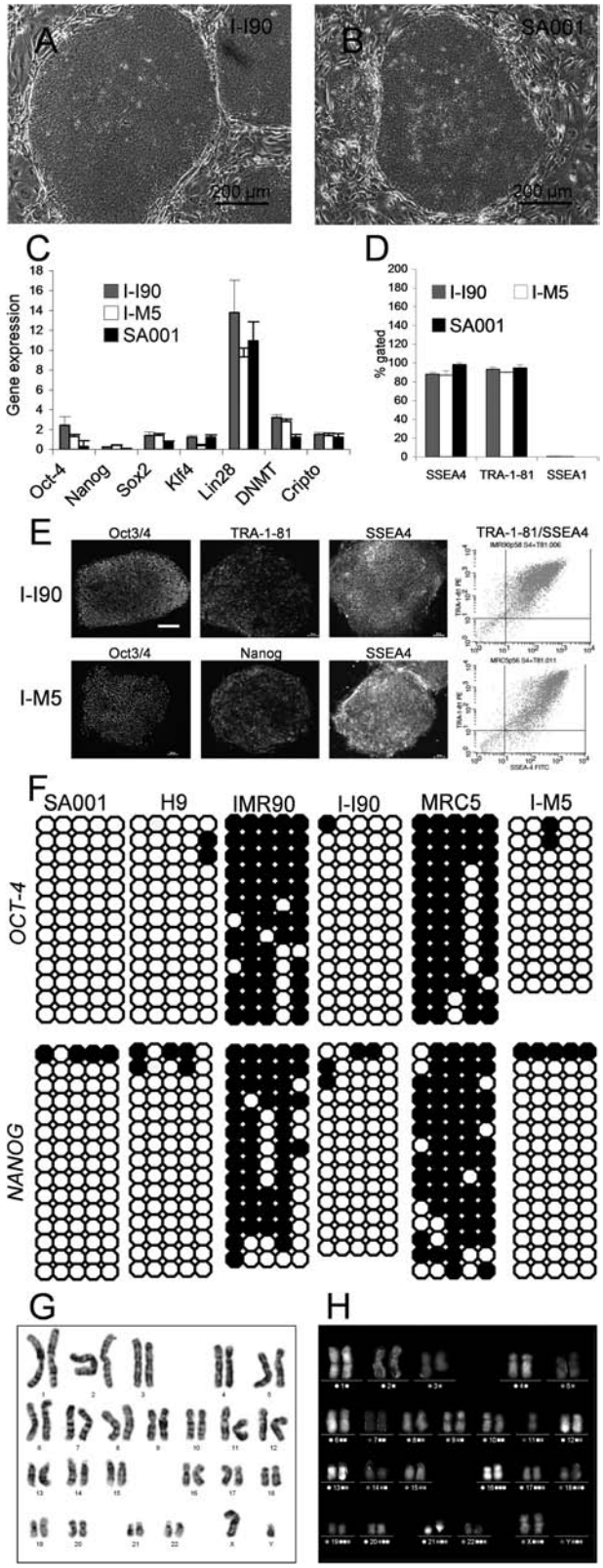

(Table 2). Nanog mRNA levels were no longer elevated in NPCs (Fig. 3H), which displayed levels of neuronal differentiation markers similar to hESC-NPCs (Fig. 3H). NPCs were uniformly labeled for Sox2 (Fig. 3D) and contained TUJ1-positive neurons (Fig. 3D) and a small proportion of GFAP astrocytes (Fig. 3E). Neuronal differentiation was confirmed with electrophysiology (Fig. 3I) (see legend). The ability of I-ShiPSC-NPCs to maintain their neuronal commitment into a rat brain environment was assessed in vitro by seeding on primary cultures of embryonic rat cortex (Fig. 3F). Neuronal differentiation was observed within 2 days (Fig. 3G).

Figure 4 depicts the global scheme of the experiments.

hiPSC-NPCs Differentiate Into GABAergic Neurons After Transplantation Into the Postischemic Brain

As previously described in this paradigm (40), 90 min MCAO resulted in a lesion restricted to the lateral quadrant of the striatum (Fig. 5A) in 65% of the animals. The other animals had larger lesions, encompassing the cortical and subcortical territories of the artery (Fig. 5B), and were not kept in the study. One month after transplantation, grafts could be identified on T2-weighted MRI (Fig. 5C) and histology (Fig. 5D). Cells were packed at injection site, with some scattered into the proximal parenchyma (Fig. 5E), and were mainly nestin positive (Fig. 5F). Grafts also contained cells positive for Sox2 (Fig. 5G) and Pax6 (Fig. 5H), but not for Oct4 (Fig. 5G), indicating sustained neural commitment in the postischemic environment. Host-graft interactions were illustrated by human MAP2 processes entering the host tissue (Fig. 5I) and by patches of host-derived tyrosine hydoxylase (TH)-positive axons (Fig. 5J) into the grafts. DARPP-32-positive neurons with an immature morphology were distributed in patches over the whole graft, indicating

FACING COLUMN

Figure 1. Validation of I-ShiPSC lines. (A, B) I-ShiPSC colonies displayed a hESC-like morphology (A: I-I90; B: SA001). (C) Quantitative PCR of self-renewal and pluripotency markers. Relative expression levels normalized to GAPDH. Mean ± SD of three independent experiments. I-ShiPSCs display no significant differences to SA001. (D) Flow cytometry for hESCs-specific cell surface markers. Levels of the pluripotency markers SSEA4 and TRA-1-81 and the differentiation marker SSEA1 in I-ShiPSCs and hESCs are similar. (E) Immunohistochemistry and FACS plots for both I-ShiPSC lines illustrating the expression of hESC-specific markers. Scale bar: 80 µm. (F) DNA methylation status of *OCT4* and *NANOG* promoter regions in hESCs, I-ShiPSC lines, and corresponding fibroblasts. Open and closed circles indicate unmethylated and methylated CpG dinucleotides, respectively. (G, H) Examples of karyotype performed with G banding (G: I-M5) and mFISH (H: I-I90) showing the absence of aneuploidy and a normal set of 46 XY (I-M5) or XX (I-I90) human chromosomes after 56 or 59 passages, respectively.

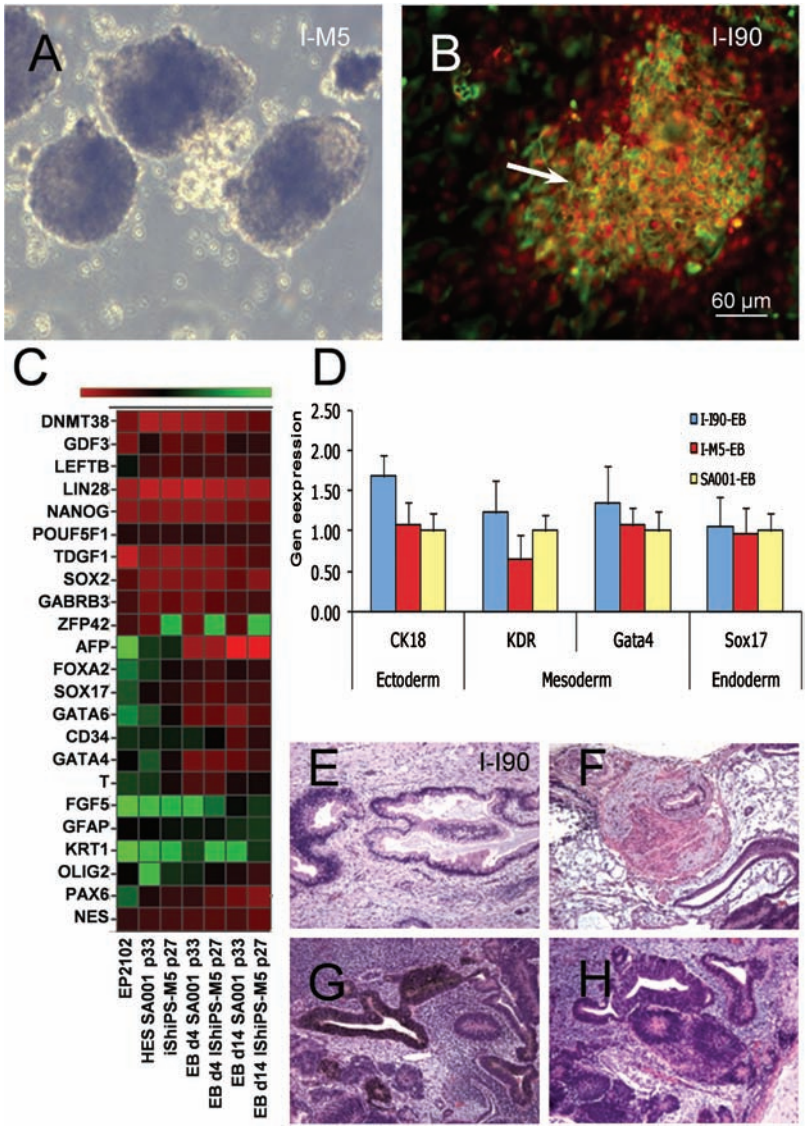

Figure 2. Assessment of I-ShiPSCs pluripotency. (A) Embryoid bodies (EBs) formed with I-M5. (B) Expression of neuron-specific class III beta-tubulin (green) and Pax6 (red) in a discrete area of an I-I90-derived EBs (day 7) showing neural differentiation. Arrow points to a neural rosette. (C) Microfluidic card of human SCs pluripotency genes; example of I-M5- and SA001-EBs at 4 and 14 days. Levels of gene expression relative to GAPDH are indicated by color changes, from red (high expression levels, low ΔCt) to green (low expression levels, high ΔCt). EP2102: control embryonal carcinoma cell line used as a reference for hESC. (D) QPCR for markers of differentiation in EBs from I-ShiPSCs and SA001 (Ectoderm: cytokeratin 18 (CK18); Mesoderm: Gata4, KDR; Endoderm: Sox17). The SA001-EBs mRNA levels are set as 1. Mean ± SD of two independent experiments. GAPDH levels were stable among cell lines: mean GAPDH Ct in EBs = 29.12 ± 1.06. (E–H) Example of teratoma derived from I-I90 showing secretory epithelium (E), smooth muscle (F), pigmented epithelium (G), and neural tissue (H). Scale bar: 250 µm.

that some NPC had initiated terminal differentiation (Fig. 5M). Similar results were obtained with SA001-NPCs (Fig. 5K, L)

After 4 months, the graft had spread into the lesion cavity, although enlargement of the lateral ventricle was still visible (Fig. 6A). Grafts formed a mixed tissue with host-derived blood vessels (Fig. 6B) and astrocytes (Fig. 6C). GABAergic striatal neurons formed clusters of fully differentiated hDARPP-32-positive neurons (Fig. 6D, E) and scattered calretinin-positive interneurons (Fig. 6F) were observed. In addition to DARPP-32, a D1-receptor-linked protein, a subpopulation of grafted neurons had type 2 dopaminergic receptors (Fig. 6G). The number of DARPP-32 neurons was not significantly different among grafts from the three cell types: SA001: 172.43 ± 7.65 cells/mm^3; I-M5: 140.59 ± 10.74 cells/mm^3; I-I90: 162 ± 13.04 cells/mm^3 (one-way ANOVA: $p = 0.84$; $F = 0.18$; dll = 19).

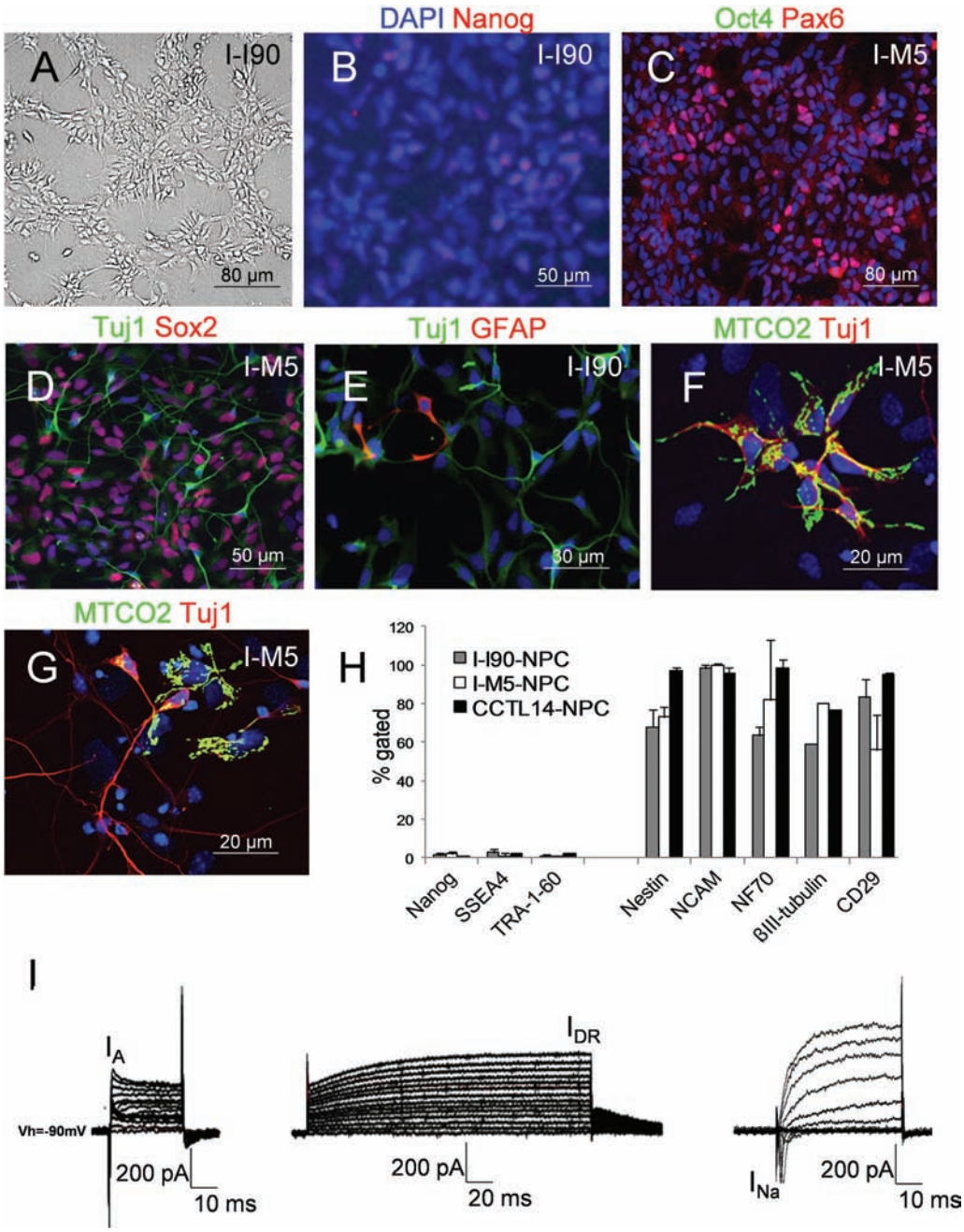

Figure 3. I-ShiPSCs differentiation into ENPs and functional NPCs. (A) ENPs form typical neural rosettes still display detectable levels of Nanog (B), express Pax6 (C) and do not express Oct4 (C). (D) After 7 days of differentiation, NPCs characterize by homogenous Sox2 expression and the presence of TUJ1-positive young neurons. (E) NPCs generate a small proportion of GFAP-positive astrocytes (2.77 ± 0.02%). (F, G) Differentiation of NPCs into young (2 days; F) and mature (5 days; G) neurons after seeding on rat cortex primary culture. (H) FACS analysis showing a similarly low expression of hESC markers (Nanog, SSEA4, TRA-1-60) and high expression of neuronal differentiation markers (Nestin, NCAM, NF70, βIII-tubulin, integrin CD29) in NPCs from I-ShiPSCs and hESCs (CCTL14 line). (I) Representative electrophysiological traces of patch-clamp recording showing fast transient current (IA) and delayed rectifier current (IDR) in ENPs. Sodium channels (INa) indicative of full neuronal maturation appear in NPCs within 5–7 days of differentiation.

Table 2. RT-PCR Quantification of mRNA Levels for hESC Genes in I-ShiPSC and SA001 hESC-Early Neural Progenitors (ENPs)

mRNA/Cell Line	SA001-ENP	I-M5-ENP	I-I90-ENP
Oct-4	0.0067 ± 0.003	0.021 ± 0.001	0.01 ± 0.004
Nanog	0.0016 ± 0.02	0.196 ± 0.14*	0.134 ± 0.07*
Sox2	0.039 ± 0.006	0.108 ± 0.07*	0.076 ± 0.027

Mean ± SD of $2^{\Delta\Delta Ct}$ normalized to GAPDH. *$p < 0.05$ compared to SA001-ENPs.

Sustained proliferation is a major side effect after grafting NPC into the lesioned striatum. Quantification of the mitotic activity with Ki67 immunoreactivity identified 2.34 ± 0.3% dividing cells in grafts at 4 months. However, the absence of colocalization with the human mitochondrial marker MTCO2 indicated that these cells were of host origin (Fig. 6H). No nonneural structures and no overgrowths were observed along the 4 months of the study.

hiPSC-NPCs Rescue Functional Impairments

Scoring of sensorimotor dysfunction (Fig. 7) with the tape removal test indicated a significant recovery of grafted animals from 2 weeks posttransplantation (Fig. 7A). Significance was maintained over the 4 months of the study, in spite of an important recovery in nongrafted animals. As reported, MCAO animals typically displayed severe long-lasting motor asymmetry in the apomorphin-induced rotation test (Fig. 7C). Grafting firstly decreased the aggravation observed between 15 and 45 days post-MCAO and, from 2 months, significantly reduced the deterioration. Baseline scores were comparable in the three groups, indicating the absence of an initial unbalance in rotation scores: SA001: 42.5 ± 24.52; I-M5: 33.6 ± 12.92; I-I90: 35.89 ± 13.18; one-way ANOVA: $p = 0.36$; $F = 1.10$; dll = 39. Other tests [Montoya staircase (Fig. 7B) and neurological scores] were not informative due to spontaneous resuming of pre-MCAO scores in nongrafted animals.

hiPSC-NPCs Project to Correct Target Areas

We used the hNCAM antibody to identify projections from grafted cells. One month after transplantation, hNCAM fibers were observed in myelinated fiber bundles of the host striatum and in the globus pallidus (Fig. 8A, B) at a maximal distance of 2 mm caudal to the injection site. No human fibers were observed in the host SN (Fig. 8C). After 2 months, human axons had extended throughout the entopedoncular nucleus (Fig. 8D, E) to the most caudal part of the SN (Fig. 8F–G). A dense graft-derived axonal network was observed in SN *pars reticulata* (SNr) (Fig. 8H), in close association to TH-positive dendrites (Fig. 8I). A few hNCAM fibers were observed in the thalamus and in the corpus callosum.

hiPS-NPCs Limit Secondary Neurodegeneration in the Host Brain

T2-weighted MRI in MCAO animals revealed a persistent atrophy of the hindbrain at the level of the SN (Fig. 9A), which was confirmed at one month by TH staining (Fig. 9B). At 1 month, MCAO animals had a reduced SNr volume on the side ipsilateral to the lesion (61.1 ± 16.8% reduction compared to nonlesioned/nongrafted animals; $p = 0.010$) (Fig. 9D). Figure 9C shows

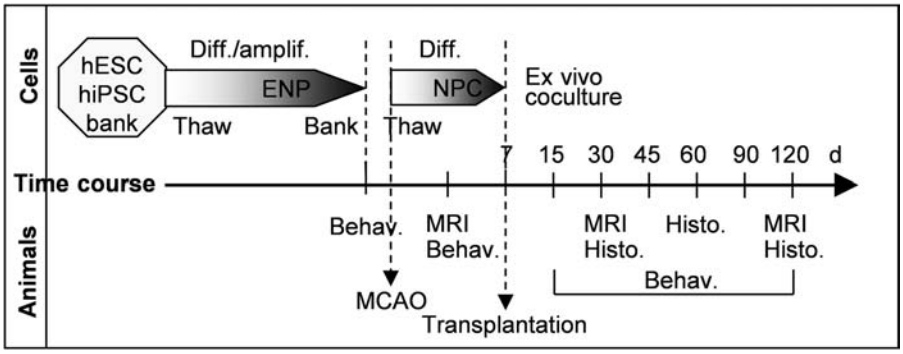

Figure 4. Schematic time course of the experiments. Experiments start with the differentiation of pluripotent SCs into ENPs and banking. ENPs are thawed when MCAO is performed and are committed to NPCs for one week before transplantation. Animals were followed with magnetic resonance imaging (MRI) and behavioral analysis over 4 months, and histological data were acquired at 1, 2, and 4 months. Diff., differentiation; amplif., amplification; Behav., behavioral analysis; Histo., histological analysis; d, days post-MCAO.

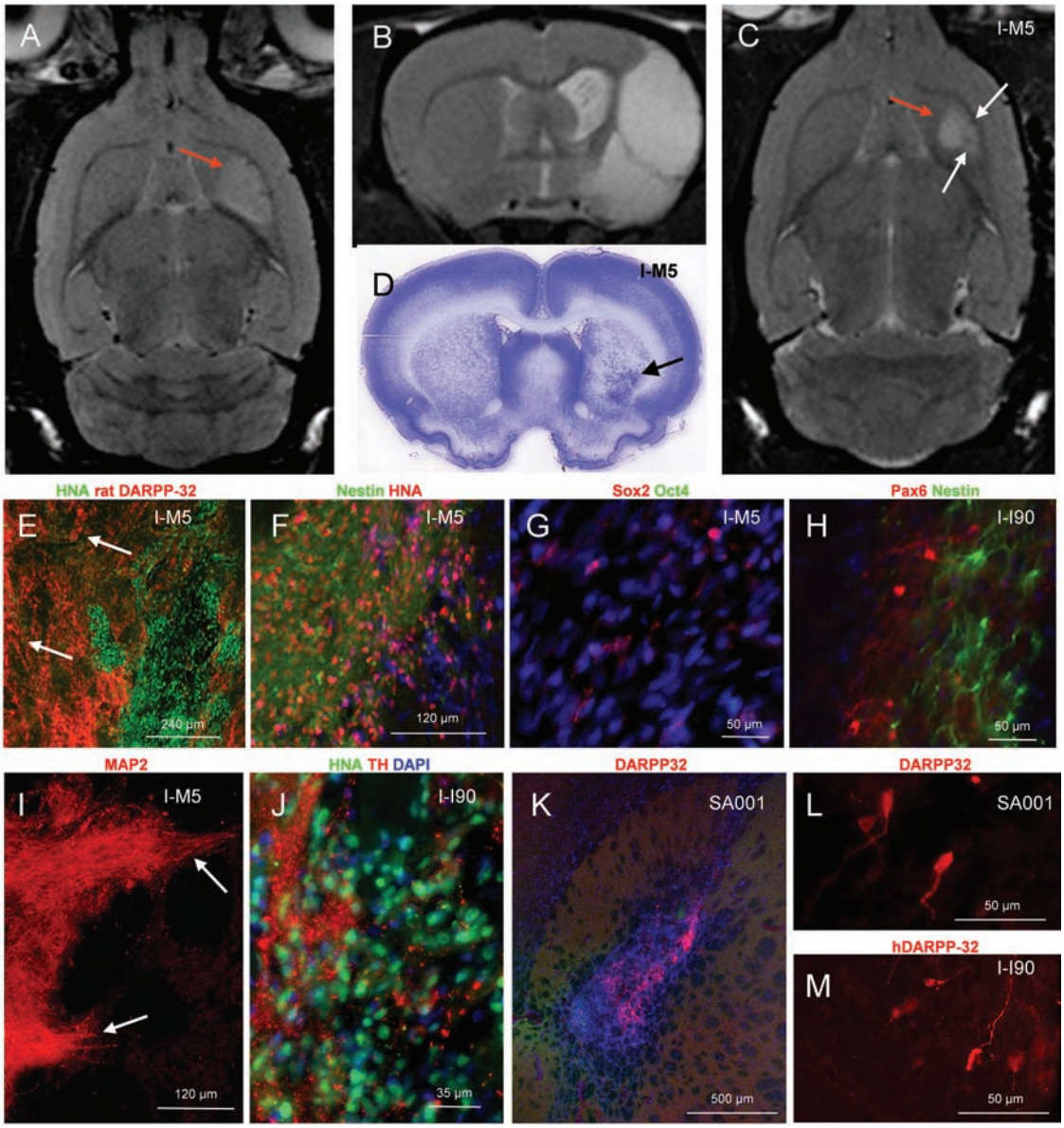

Figure 5. One month posttransplantation. (A) Animals with lesions restricted to the striatum were used in this study. (B) Animals with larger lesions were excluded. (C) The lesion (red arrow) and graft (white arrows) are distinguished on T2-weighed MRI by their intensity. (D) Postmortem histology shows the graft (arrow) in the lateral quadrant of the striatum. (E) Clusters of human (HNA) cells (arrows) have migrated away from injection site into the perilesional host parenchyma, although on short distances. Grafts contain a majority of nestin- (F), Sox2-, but no Oct4-positive cells (G), and small clusters of Pax6 cells (H). MAP2 processes originating from the graft gather into bundles to enter the host parenchyma (I, arrows). Grafts also contained TH-labeled fibers (J) and a small number of immature DARPP-32 neurons (L, M). (K) SA001-NPCgrafts had similar features, with clusters of immature DARPP-32 neurons (L).

that variations among the three groups (SA001-NPCs, I-I90-NPCs, I-M5-NPCs) were not significant [one-way ANOVA: SN pars compacta (SNc): $p = 0.66$, $F = 0.43$, dll = 17; SNr $p = 0.59$, $F = 0.54$, dll = 17). Grafting reduced the atrophy of pars reticulata to $27.13 \pm 11.50\%$ (Fig. 9D) ($p = 0.017$, $t = 2.26$, dll = 8). MCAO-induced reduction of the volume occupied by TH cell bodies in pars compacta was not significant. However, nonbiased stereological quantification of TH-positive cell bodies (Fig. 9E) indicated a $46.20 \pm 12.41\%$ loss of TH neurons after MCAO ($p = 0.03$), reduced to a $21.11 \pm 6.65\%$ loss after grafting ($p = 0.02$) (Fig. 9F), corresponding to a 47% protection.

DISCUSSION

This study shows that intracerebral transplantation of hiPSC-NPCs in the subacute phase of cerebral ischemia has the potential to reverse functional deficits and to limit

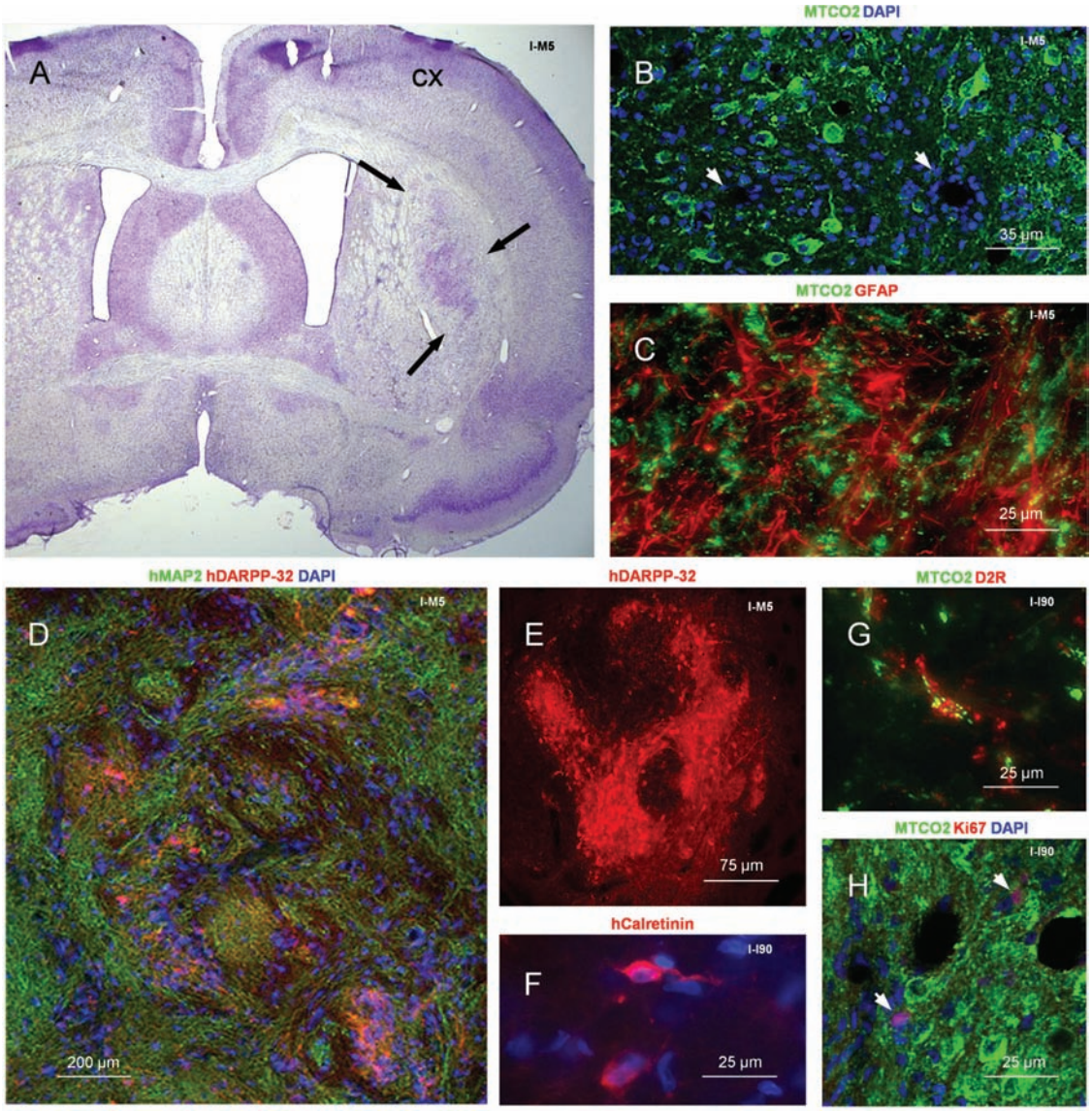

Figure 6. Four months posttransplantation. (A) Cresyl violet staining showing the graft in the lateral striatum (black arrows). Grafts formed a mixed tissue with the host, with MTCO2-negative (B; arrow heads) endothelial cells and astrocytes (C). (D–F) Grafts contained large clusters of DARPP-32 projection neurons (D, E), calretinin interneurons (F), and neurons with D2 dopaminergic receptors (G). (H) Ki67 labeling showing dividing cells (arrow heads) of rat (MTCO2-negative) origin.

degeneration of remote brain structures connected to the lesion site.

On the cell biology aspect, this study firstly confirmed that hiPSC and hESC can respond to the same differentiation protocol. NPCs were derived according to the dual-SMAD inhibitor protocol developed for hESCs, based on the inhibition of nodal/activin and BMP signaling pathways and resulting in accelerated commitment of pluripotent SCs (PSCs) into NSCs (8). A main advantage of the NSC protocol is the rapid production of large pools of homogenous NPCs after 5–7 days of differentiation from frozen stocks. This protocol reduces individual differences in neural commitment among PSCs (8).

Effective cell replacement therapy critically relies on the ability of transplanted progenitors to generate neurons with topographically relevant phenotypes. Striatal stroke induces massive loss of medium spiny GABAergic neurons, leading to the disruption of the striatonigral loop. As described for hESC-NPCs in this model (6,42), grafted hiPSC-NPCs accurately generated long-projection GABAergic neurons characterized by the D1 receptor second messenger DARPP-32. The low percentage of DARPP-32

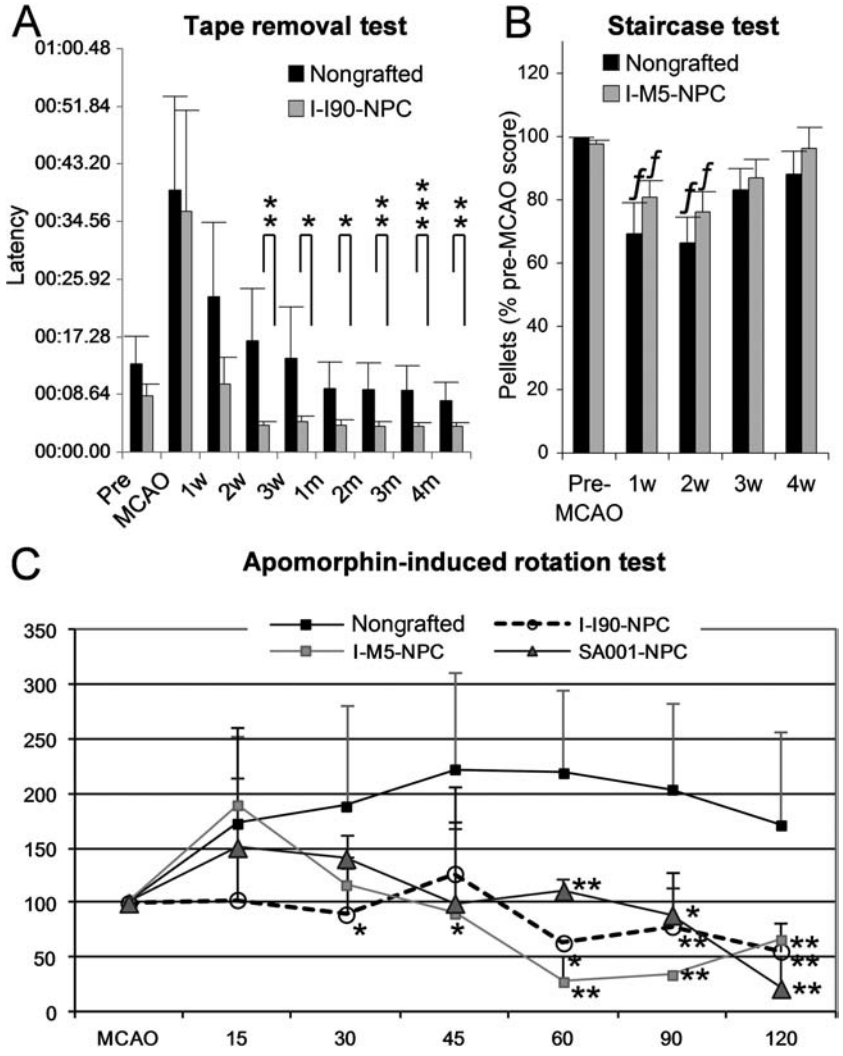

Figure 7. Transplantation improves functional recovery. (A) Adhesive removal test for I-I90-NPCs-grafted animals show a complete recovery from the second week postgrafting (w, week; m, month). (B) Staircase test for I-M5-NPC-grafted animals show rapid spontaneous recovery in the nongrafted group; w, week postgrafting. *f*, $p<0.05$ compared to the pre-MCAO score in the corresponding group. (C) Apomorphin-induced rotation in nongrafted animals and animals grafted with NPC from I-M5, I-I90, and SA001. Scores are represented as percentage of MCAO baseline data. One-way ANOVA with Bonferroni–Dunn test for intergroups comparison at each experimental step. $^{**}p<0.01$, $^{*}p<0.05$.

neurons observed in grafts can be attributed to the lack of particular commitment during NPC differentiation and might be improved by specific differentiation protocols.

The second requirement for cell replacement therapy is accurate reconstruction of disrupted pathways (13). The ability of human neural progenitors to extend axons into the adult rat brain was first described by Wictorin and collaborators after excitotoxic striatal lesion (51). Subsequent studies have histologically (19) and electrophysiologically (6,11,19) reported synaptic contacts between human NPCs and the adult rodent brain in stroke models. The possibility for human grafted neurons to form long-distance axonal projections is less documented and controversial. On one hand, few retrogradely labeled axons were observed in cortical transplants after injection of a tracer into the thalamus (16). Limited projection from grafted cortical tissue and the underlying striatum was reported in a model of cortical ischemia (44). On the other hand, Gaillard et al. observed specific connections between murine homotopic nigral transplants and the host striatum in a model of Parkinson's disease (14) and from murine ESC-NPCs intracortical transplants to the host spinal cord (15). Reconstruction of the striatonigral loop was also achieved by simultaneous intrastriatal and intranigral grafting (31). A major result of our study was the fact that grafted hiPSC-NPCs extended axons toward

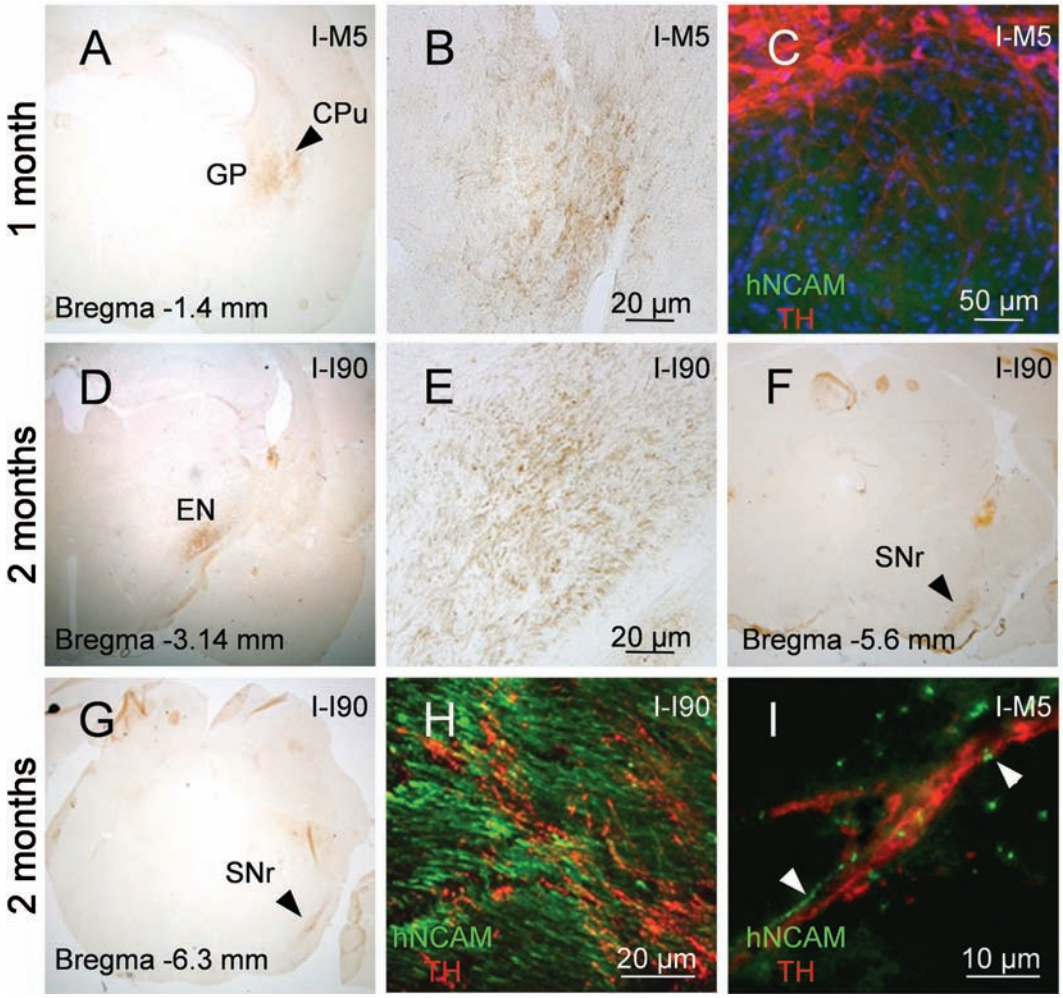

Figure 8. I-ShiPS-NPCs project axons into the host brain. (A, B) After 1 month, human fibers were seen in the host globus pallidus (GP). CPu, caudate putamen nucleus. (C) No hNCAM-labeled fibers were seen in the SN. (D–I) Graft-derived axonal elongation at 2 months. Axons are seen in the entopeduncular nucleus (D, E) and the SN (F, G) down to its caudalmost part (G). (H) Human axons intermingled with host TH-positive axons from the SN pars compacta at the entry of SN. (I) Graft-derived axons (green) in close apposition to dopaminergic neuron dendrites (red) in pars reticulata.

the remote host SN with great specificity. This suggests that hiPSC-NPCs have the potential to recognize their target over long distances in the adult postischemic brain. The molecular content of the dialogue that establishes between grafted cells and the recipient brain remains to be understood. It might relate to the particularly prone-to-remodeling state of the poststroke brain (32). Alternatively, axonal extension in a xenograft situation might result from an insensibility of human axons to the adult rat brain inhibitory molecules (41) that would normally prevent the growth of rat axons. Reciprocity of this dialogue was suggested by the rapid sprouting of host-derived TH fibers into the grafts. The importance of host afferents in graft development has been emphasized in previous studies (12,29) and could have played a role in guiding the terminal differentiation of grafted neurons.

For cell replacement to be causally linked to restoration of impaired functions, a temporal relationship should have existed between the maturation of graft-derived GABAergic neurons in the host striatum and the kinetics of functional recovery. However, improvements of sensorimotor functions in the adhesive removal test occurred very rapidly and were temporally dissociated from both the maturation of GABAergic neurons in grafts and axonal projections to host target areas, which occurred weeks later. This temporal discrepancy suggests the existence of mechanisms unrelated to the maturation and integration of grafted cells. Non cell-autonomous mechanisms have been evoked as major mediators of SCs effects in stroke, including with NPCs (5,26,35,36,38,43,53). They are commonly attributed to the release, by immature exogenous cells,

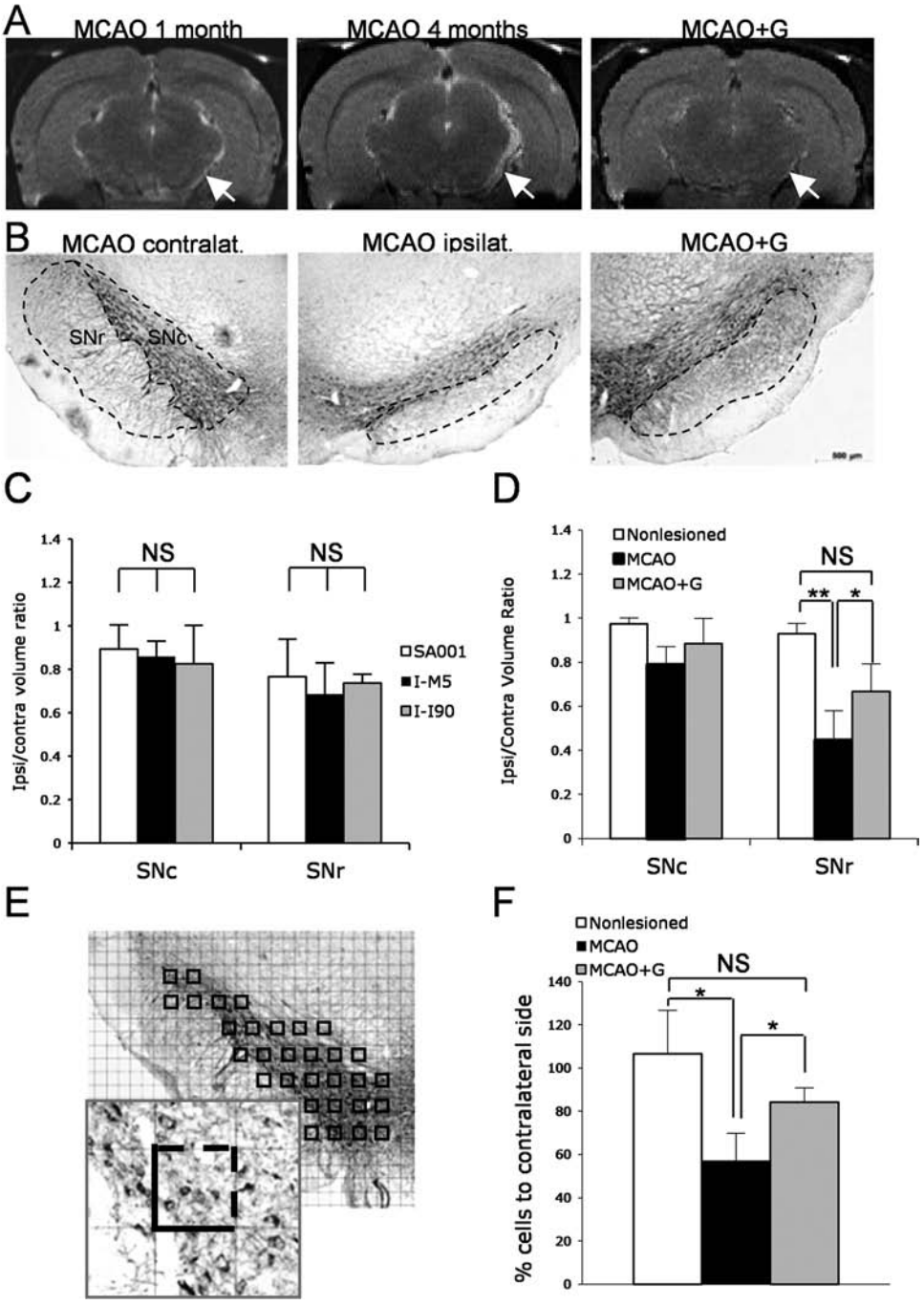

Figure 9. Transplantation prevents substantia nigra atrophy. (A) T2 weighted MRI shows a global atrophy of the right side (arrows) in a lesioned animal (MCAO) at 1 and 4 months post-MCAO, which is less conspicuous in grafted animals (MCAO+G; example of I-I90-NPCs graft). (B) Anti-TH immunohistochemistry in SN pars compacta (SNc) and pars reticulata (SNr) at 1 month. Delineation shows the area for volumetric measures. (C) Quantification of SNr and SNc volumes in animals grafted with the three lines-NPCs confirmed the homogeneity of the groups. (D) Grafting (MCAO+G) significantly reduce SNr atrophy induced by MCAO. $*p<0.05$. (E) Illustration of the sampling for TH neuron counting. Insert shows the counting frame. Counts included neurons with visible nucleus present inside the frame or crossing the dashed line. (F) Quantification of TH-positive neurons in SNc, showing stroke-induced reduction and protection by grafting. One-way ANOVA with Bonferroni–Dunn test, $*p<0.05$. NS, nonstatistically significant.

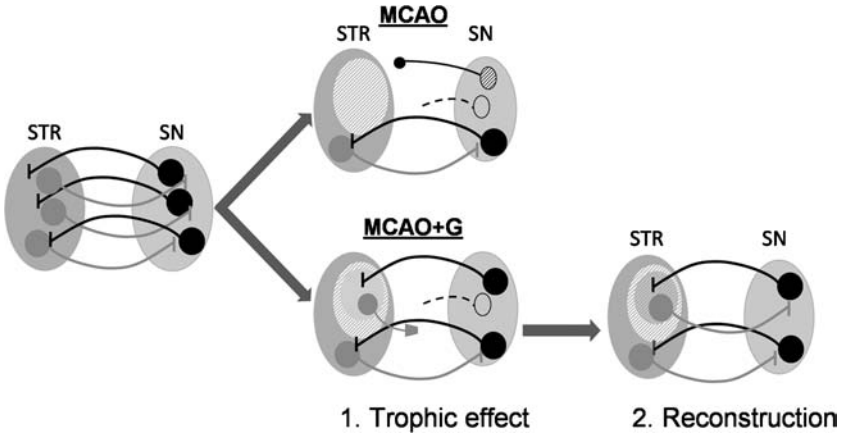

Figure 10. Suggested effects of hiPSC-NPCs grafted into the postischemic brain. Reciprocal connections link the substantia nigra (SN) to the striatum (STR). Stroke (MCAO) depletes the STR neuronal populations and deprives SN of both afferent and target cells, resulting in atrophy and partial cell death (no graft). Grafting (MCAO+Graft) firstly rescues the atrophy by providing SN striatal afferents with new targets and by promoting SN axonal sprouting (1. Trophic effect). Secondly, with maturation of transplanted cells, reconstruction of the STR-SN loop allows maintenance of functions (2. Reconstruction).

of neuroprotective, antioxidant, and anti-inflammatory molecules that can both limit degeneration and improve the structural reorganization of the post-stroke brain. The characterization of this dialogue in our paradigm deserves further investigations.

In contrast with the rapid recovery of sensorimotor functions, improvements of motor ability in the apomorphin-induced test established slowly. Apomorphin is an agonist of dopaminergic receptors that requires maturation of striatal neurons to be effective. The time course of motor recovery in this test nicely corresponded to the maturation of DARPP-32 neurons and to axonal projection to the SN.

Secondary alteration in areas functionally related to the lesion site after stroke has been described in patients (50) and animal models (33,46) and greatly contributes to long-term functional impairments. The reduction of TH fibers in the striatum directly correlates with the atrophy of the SN (22), and striatal administration of trophic factors after lesion of SN axons protects against SN degeneration. In addition, intrastriatal grafting of mesenchymal SCs reduced the sensitivity of SN neurons to the toxicity of 6-hydroxydopamine (4,37), showing that SCs can exert a protective effect on SN neurons. We propose that the trophic effect exerted on host SN afferents by the graft was instrumental in promoting TH afferent sprouting into the graft and protecting the SN from atrophy, leading to rapid restoration of sensorimotor functions.

CONCLUSIONS

The driving force of current SC therapy research is to achieve a comprehensive understanding of the mechanisms by which transplanted cells restore lost functions. So far, reported mechanisms include bystander effects nonrelated to intracerebral integration of exogenous cells and effects that directly rely on this integration. Due to its pathogenic characteristics, stroke can uniquely benefit from this duality. In the acute phase, cell death and inflammation predominates and trophic, angiogenic, and/or anti-inflammatory actions can reduce the severity of infarction without cell engraftment. In contrast, the post-acute and chronic phases are times for intense axonal and synaptic reorganization that can be efficiently supported by integrated cells. As schematized in Figure 10, hiPSC-NPCs might act both rapidly with unspecific trophic effects and, secondarily, through integration and reconstruction of connections with host structures. A final step is needed before hiPSC-derived progenies enter the clinic, which relies on improvements of both the quality (to limit genetic and epigenetic modifications) and the availability of cells. The production of "patient-tailored" hiPSC, which could avoid transplant rejection, is a months-taking procedure and might not fit with the emergency requirements of stroke treatment. In contrast, the iPSC strategy allows the derivation of HLA-compatible cell banks that might provide the ideal cell source for cell replacement therapy or more generally SC therapy in stroke.

ACKNOWLEDGMENTS: We thank C. André for teratoma formation and analysis, X. Nissan for qPCR, M. Feyeux for cell culture, C. Varella for karyotyping, N. Lefort for FACS, and A. Günther-Kern and I. Heinemann for animal surgery and staircase testing. This work was performed in and granted by the STEMS ("Preclinical analysis of stem cell therapy for stroke") FP6 European project. It was supported by the Association Française contre les Myopathies (AFM) and the grant 1M0538 from the Ministry of Education, Youth, and Sports of the Czech Republic. The authors declare no conflicts of interest.

REFERENCES

1. Andrey, P.; Maurin, Y. Free-D: An integrated environment for three-dimensional reconstruction from serial sections. J. Neurosci. Methods 145(1–2):233–244; 2005.
2. Arvidsson, A.; Kirik, D.; Lundberg, C.; Mandel, R. J.; Andsberg, G.; Kokaia, Z.; Lindvall, O. Elevated GDNF levels following viral vector-mediated gene transfer can increase neuronal death after stroke in rats. Neurobiol. Dis. 14(3):542–556; 2003.
3. Bang, O. Y.; Lee, J. S.; Lee, P. H.; Lee, G. Autologous mesenchymal stem cell transplantation in stroke patients. Ann. Neurol. 57(6):874–882; 2005.
4. Blandini, F.; Cova, L.; Armentero, M. T.; Zennaro, E.; Levandis, G.; Bossolasco, P.; Calzarossa, C.; Mellone, M.; Giuseppe, B.; Deliliers, G. L.; Polli, E.; Nappi, G.; Silani, V. Transplantation of undifferentiated human mesenchymal stem cells protects against 6-hydroxydopamine neurotoxicity in the rat. Cell Transplant. 19(2):203–217; 2010.
5. Bliss, T. M.; Andres, R. H.; Steinberg, G. K. Optimizing the success of cell transplantation therapy for stroke. Neurobiol. Dis. 37(2):275–283; 2010.
6. Buhnemann, C.; Scholz, A.; Bernreuther, C.; Malik, C. Y.; Braun, H.; Schachner, M.; Reymann, K. G.; Dihne, M. Neuronal differentiation of transplanted embryonic stem cell-derived precursors in stroke lesions of adult rats. Brain 129(Pt 12):3238–3248; 2006.
7. Burns, T. C.; Verfaillie, C. M.; Low, W. C. Stem cells for ischemic brain injury: A critical review. J. Comp. Neurol. 515(1):125–144; 2009.
8. Chambers, S. M.; Fasano, C. A.; Papapetrou, E. P.; Tomishima, M.; Sadelain, M.; Studer, L. Highly efficient neural conversion of human ES and iPS cells by dual inhibition of SMAD signaling. Nat. Biotechnol. 27(3):275–280; 2009.
9. Chen, S. J.; Chang, C. M.; Tsai, S. K.; Chang, Y. L.; Chou, S. J.; Huang, S. S.; Tai, L. K.; Chen, Y. C.; Ku, H. H.; Li, H. Y.; Chiou, S. H. Functional improvement of focal cerebral ischemia injury by subdural transplantation of induced pluripotent stem cells with fibrin glue. Stem Cells Dev. 19(11):1757–1767; 2010.
10. Chopp, M.; Steinberg, G. K.; Kondziolka, D.; Lu, M.; Bliss, T. M.; Li, Y.; Hess, D. C.; Borlongan, C. V. Who's in favor of translational cell therapy for stroke: STEPS forward please? Cell Transplant. 18(7):691–693; 2009.
11. Daadi, M. M.; Li, Z.; Arac, A.; Grueter, B. A.; Sofilos, M.; Malenka, R. C.; Wu, J. C.; Steinberg, G. K. Molecular and magnetic resonance imaging of human embryonic stem cell-derived neural stem cell grafts in ischemic rat brain. Mol. Ther. 17(7):1282–1291; 2009.
12. Defontaines, B.; Peschanski, M.; Onteniente, B. Host dopaminergic afferents affect the development of DARPP-32 immunoreactivity in transplanted embryonic striatal neurons. Neuroscience 48(4):857–869; 1992.
13. Dihne, M.; Hartung, H. P.; Seitz, R. J. Restoring neuronal function after stroke by cell replacement: Anatomic and functional considerations. Stroke 42(8):2342–2350; 2011.
14. Gaillard, A.; Decressac, M.; Frappe, I.; Fernagut, P. O.; Prestoz, L.; Besnard, S.; Jaber, M. Anatomical and functional reconstruction of the nigrostriatal pathway by intranigral transplants. Neurobiol. Dis. 35(3):477–488; 2009.
15. Gaillard, A.; Prestoz, L.; Dumartin, B.; Cantereau, A.; Morel, F.; Roger, M.; Jaber, M. Reestablishment of damaged adult motor pathways by grafted embryonic cortical neurons. Nat. Neurosci. 10(10):1294–1299; 2007.
16. Gonzalez, M. F.; Sharp, F. R.; Loken, J. E. Fetal frontal cortex transplanted to injured motor/sensory cortex of adult rats: Reciprocal connections with host thalamus demonstrated with WGA-HRP. Exp. Neurol. 99(1):154–165; 1988.
17. Gore, A.; Li, Z.; Fung, H. L.; Young, J. E.; Agarwal, S.; Antosiewicz-Bourget, J.; Canto, I.; Giorgetti, A.; Israel, M. A.; Kiskinis, E.; Lee, J. H.; Loh, Y. H.; Manos, P. D.; Montserrat, N.; Panopoulos, A. D.; Ruiz, S.; Wilbert, M. L.; Yu, J.; Kirkness, E. F.; Izpisua Belmonte, J. C.; Rossi, D. J.; Thomson, J. A.; Eggan, K.; Daley, G. Q.; Goldstein, L. S.; Zhang, K. Somatic coding mutations in human induced pluripotent stem cells. Nature 471(7336):63–67; 2011.
18. Hicks, A.; Schallert, T.; Jolkkonen, J. Cell-based therapies and functional outcome in experimental stroke. Cell Stem Cell 5(2):139–140; 2009.
19. Ishibashi, S.; Sakaguchi, M.; Kuroiwa, T.; Yamasaki, M.; Kanemura, Y.; Shizuko, I.; Shimazaki, T.; Onodera, M.; Okano, H.; Mizusawa, H. Human neural stem/progenitor cells, expanded in long-term neurosphere culture, promote functional recovery after focal ischemia in Mongolian gerbils. J. Neurosci. Res. 78(2):215–223; 2004.
20. Kawai, H.; Yamashita, T.; Ohta, Y.; Deguchi, K.; Nagotani, S.; Zhang, X.; Ikeda, Y.; Matsuura, T.; Abe, K. Tridermal tumorigenesis of induced pluripotent stem cells transplanted in ischemic brain. J. Cereb. Blood Flow Metab. 30(8):1487–1493; 2010.
21. Kim, K.; Doi, A.; Wen, B.; Ng, K.; Zhao, R.; Cahan, P.; Kim, J.; Aryee, M. J.; Ji, H.; Ehrlich, L. I.; Yabuuchi, A.; Takeuchi, A.; Cunniff, K. C.; Hongguang, H.; McKinney-Freeman, S.; Naveiras, O.; Yoon, T. J.; Irizarry, R. A.; Jung, N.; Seita, J.; Hanna, J.; Murakami, P.; Jaenisch, R.; Weissleder, R.; Orkin, S. H.; Weissman, I. L.; Feinberg, A. P.; Daley, G. Q. Epigenetic memory in induced pluripotent stem cells. Nature 467(7313):285–290; 2010.
22. Kirik, D.; Rosenblad, C.; Bjorklund, A. Characterization of behavioral and neurodegenerative changes following partial lesions of the nigrostriatal dopamine system induced by intrastriatal 6-hydroxydopamine in the rat. Exp. Neurol. 152(2):259–277; 1998.
23. Kiskinis, E.; Eggan, K. Progress toward the clinical application of patient-specific pluripotent stem cells. J. Clin. Invest. 120(1):51–59; 2010.
24. Kondziolka, D.; Steinberg, G. K.; Wechsler, L.; Meltzer, C. C.; Elder, E.; Gebel, J.; Decesare, S.; Jovin, T.; Zafonte, R.; Lebowitz, J.; Flickinger, J. C.; Tong, D.; Marks, M. P.; Jamieson, C.; Luu, D.; Bell-Stephens, T.; Teraoka, J. Neurotransplantation for patients with subcortical motor stroke: A phase 2 randomized trial. J. Neurosurg. 103(1): 38–45; 2005.
25. Lapillonne, H.; Kobari, L.; Mazurier, C.; Tropel, P.; Giarratana, M. C.; Zanella-Cleon, I.; Kiger, L.; Wattenhofer-Donze, M.; Puccio, H.; Hebert, N.; Francina, A.; Andreu, G.; Viville, S.; Douay, L. Red blood cell generation from human induced pluripotent stem cells: Perspectives for transfusion medicine. Haematologica 95(10):1651–1659; 2010.
26. Lee, J. P.; Jeyakumar, M.; Gonzalez, R.; Takahashi, H.; Lee, P. J.; Baek, R. C.; Clark, D.; Rose, H.; Fu, G.; Clarke, J.; McKercher, S.; Meerloo, J.; Muller, F. J.; Park, K. I.; Butters, T. D.; Dwek, R. A.; Schwartz, P.; Tong, G.; Wenger, D.; Lipton, S. A.; Seyfried, T. N.; Platt, F. M.; Snyder, E. Y. Stem cells act through multiple mechanisms to benefit mice with neurodegenerative metabolic disease. Nat. Med. 13(4):439–447; 2007.

27. Lindvall, O.; Kokaia, Z. Stem cells in human neurodegenerative disorders—time for clinical translation? J. Clin. Invest. 120(1):29–40; 2010.
28. Lister, R.; Pelizzola, M.; Kida, Y. S.; Hawkins, R. D.; Nery, J. R.; Hon, G.; Antosiewicz-Bourget, J.; O'Malley, R.; Castanon, R.; Klugman, S.; Downes, M.; Yu, R.; Stewart, R.; Ren, B.; Thomson, J. A.; Evans, R. M.; Ecker, J. R. Hotspots of aberrant epigenomic reprogramming in human induced pluripotent stem cells. Nature 471(7336):68–73; 2011.
29. Liu, F. C.; Dunnett, S. B.; Graybiel, A. M. Influence of mesostriatal afferents on the development and transmitter regulation of intrastriatal grafts derived from embryonic striatal primordia. J. Neurosci. 12(11):4281–4297; 1992.
30. Longa, E. Z.; Weinstein, P. R.; Carlson, S.; Cummins, R. Reversible middle cerebral artery occlusion without craniectomy in rats. Stroke 20(1):84–91; 1989.
31. Mendez, I.; Sadi, D.; Hong, M. Reconstruction of the nigrostriatal pathway by simultaneous intrastriatal and intranigral dopaminergic transplants. J. Neurosci. 16(22): 7216–7227; 1996.
32. Moskowitz, M. A.; Lo, E. H.; Iadecola, C. The science of stroke: Mechanisms in search of treatments. Neuron 67(2):181–198; 2010.
33. Nakane, M.; Teraoka, A.; Asato, R.; Tamura, A. Degeneration of the ipsilateral substantia nigra following cerebral infarction in the striatum. Stroke 23(3):328–332; 1992.
34. Nakatsuji, N.; Nakajima, F.; Tokunaga, K. HLA-haplotype banking and iPS cells. Nat. Biotechnol. 26(7):739–740; 2008.
35. Onteniente, B.; Polentes, J. Regenerative medicine for stroke—are we there yet? Cerebrovasc. Dis. 31(6):544–551; 2011.
36. Ramos-Cabrer, P.; Justicia, C.; Wiedermann, D.; Hoehn, M. Stem cell mediation of functional recovery after stroke in the rat. PLoS One 5(9):e12779; 2010.
37. Rosenblad, C.; Kirik, D.; Devaux, B.; Moffat, B.; Phillips, H. S.; Bjorklund, A. Protection and regeneration of nigral dopaminergic neurons by neurturin or GDNF in a partial lesion model of Parkinson's disease after administration into the striatum or the lateral ventricle. Eur. J. Neurosci. 11(5):1554–1566; 1999.
38. Sanberg, P. R.; Eve, D. J.; Willing, A. E.; Garbuzova-Davis, S.; Tan, J.; Sanberg, C. D.; Allickson, J. G.; Cruz, L. E.; Borlongan, C. V. The treatment of neurodegenerative disorders using umbilical cord blood and menstrual blood-derived stem cells. Cell Transplant. 20(1):85–94; 2011.
39. Schallert, T.; Woodlee, M. T.; Fleming, S.M. Disentangling multiple types of recovery from brain injury. In: Krieglstein, J.; Klumpp, S., eds. Pharmacology of Cerebral Ischemia. Stuttgart, Germany: Medpharm Scientific Publishers; 2012:201–216
40. Schmid-Elsaesser, R.; Zausinger, S.; Hungerhuber, E.; Baethmann, A.; Reulen, H. J. A critical reevaluation of the intraluminal thread model of focal cerebral ischemia: Evidence of inadvertent premature reperfusion and subarachnoid hemorrhage in rats by laser-Doppler flowmetry. Stroke 29(10):2162–2170; 1998.
41. Schwab, M. E.; Kapfhammer, J. P.; Bandtlow, C. E. Inhibitors of neurite growth. Annu. Rev. Neurosci. 16:565–595; 1993.
42. Seminatore, C.; Polentes, J.; Ellman, D.; Kozubenko, N.; Itier, V.; Tine, S.; Tritschler, L.; Brenot, M.; Guidou, E.; Blondeau, J.; Lhuillier, M.; Bugi, A.; Aubry, L.; Jendelova, P.; Sykova, E.; Perrier, A. L.; Finsen, B.; Onteniente, B. The postischemic environment differentially impacts teratoma or tumor formation after transplantation of human embryonic stem cell-derived neural progenitors. Stroke 41(1):153–159; 2010.
43. Shimada, I. S.; Spees, J. L. Stem and progenitor cells for neurological repair: Minor issues, major hurdles, and exciting opportunities for paracrine-based therapeutics. J. Cell. Biochem. 112(2):374–380; 2011.
44. Sorensen, J. C.; Grabowski, M.; Zimmer, J.; Johansson, B. B. Fetal neocortical tissue blocks implanted in brain infarcts of adult rats interconnect with the host brain. Exp. Neurol. 138(2):227–235; 1996.
45. Takahashi, K.; Yamanaka, S. Induction of pluripotent stem cells from mouse embryonic and adult fibroblast cultures by defined factors. Cell 126(4):663–676; 2006.
46. Tamura, A.; Kirino, T.; Sano, K.; Takagi, K.; Oka, H. Atrophy of the ipsilateral substantia nigra following middle cerebral artery occlusion in the rat. Brain Res. 510(1):154–157; 1990.
47. Tang, Y.; Yasuhara, T.; Hara, K.; Matsukawa, N.; Maki, M.; Yu, G.; Xu, L.; Hess, D. C.; Borlongan, C. V. Transplantation of bone marrow-derived stem cells: A promising therapy for stroke. Cell Transplant. 16(2):159–169; 2007.
48. Tchieu, J.; Kuoy, E.; Chin, M. H.; Trinh, H.; Patterson, M.; Sherman, S. P.; Aimiuwu, O.; Lindgren, A.; Hakimian, S.; Zack, J. A.; Clark, A. T.; Pyle, A. D.; Lowry, W. E.; Plath, K. Female human iPSCs retain an inactive X chromosome. Cell Stem Cell 7(3):329–342; 2010.
49. van Gijn, J.; Dennis, M. S. Issues and answers in stroke care. Lancet 352 Suppl 3:SIII23–27; 1998.
50. Volpe, B. T.; Blau, A. D.; Wessel, T. C.; Saji, M. Delayed histopathological neuronal damage in the substantia nigra compacta (nucleus A9) after transient forebrain ischaemia. Neurobiol Dis. 2(2):119–127; 1995.
51. Wictorin, K.; Ouimet, C. C.; Bjorklund, A. Intrinsic organization and connectivity of intrastriatal striatal transplants in rats as revealed by DARPP-32 immunohistochemistry: Specificity of connections with the lesioned host brain. Eur. J. Neurosci. 1(6):690–701; 1989.
52. Yu, J.; Vodyanik, M. A.; Smuga-Otto, K.; Antosiewicz-Bourget, J.; Frane, J. L.; Tian, S.; Nie, J.; Jonsdottir, G. A.; Ruotti, V.; Stewart, R.; Slukvin, II; Thomson, J. A. Induced pluripotent stem cell lines derived from human somatic cells. Science 318(5858):1917–1920; 2007.
53. Zhang, Z. G.; Chopp, M. Neurorestorative therapies for stroke: Underlying mechanisms and translation to the clinic. Lancet Neurol. 8(5):491–500; 2009.